POLITECNICO DI TORINO
Repository ISTITUZIONALE

Numerical simulations of small amplitude oscillatory shear flow of suspensions of rigid particles in non-Newtonian liquids at finite inertia

(Article begins on next page)

05 February 2025

OKINAWA INSTITUTE OF SCIENCE AND TECHNOLOGY

Numerical simulations of small amplitude oscillatory shear flow of suspensions of rigid particles in non-Newtonian liquids at finite inertia

Numerical simulations of small amplitude oscillatory shear flow of suspensions of rigid particles in non-Newtonian liquids at finite inertia

Massimiliano M. Villone,[1, a)] Marco E. Rosti,[2] Outi Tammisola,[3] and Luca Brandt[3]

[1)] *Dipartimento di Ingegneria Chimica, dei Materiali e della Produzione Industriale,*
Università degli Studi di Napoli Federico II, P.le Tecchio 80, 80125 Napoli,
Italy
[2)] *Complex Fluids and Flows Unit, Okinawa Institute of Science and Technology Graduate University, 1919-1 Tancha,*
Onna-son, Okinawa 904-0495, Japan
[3)] *Linné FLOW Centre and SeRC, KTH Mechanics, Osquars Backe 18, SE-100 44 Stockholm,*
Sweden

We perform immersed-boundary-method numerical simulations of small amplitude oscillatory shear (SAOS) flow of suspensions of mono-disperse non-colloidal rigid spherical particles in non-Newtonian liquids from the dilute to the concentrated regime. We study the influence of suspending liquid inertia and rheology and particle concentration on the computationally measured storage and loss moduli of the suspensions. In particular, the rheology of the suspending liquid is modeled through the inelastic shear-thinning Carreau-Yasuda constitutive equation and the viscoelastic Giesekus and Oldroyd-B constitutive equations. The role of inertia is quantified by the Stokes number, St, whereas the relevance of the non-Newtonian effects of the suspension matrix is measured through the Carreau number, Cu, for the Carreau-Yasuda liquid and through the Deborah number, De, for the viscoelastic liquids. In suspensions with a Carreau-Yasuda matrix, both the storage and the loss modulus increase with St and decrease with Cu, yet the order of magnitude of Cu has to be greater than unity for these effects to be visible. In suspensions with a viscoelastic matrix, both the moduli increase with St and have a non-monotonic trend with De, showing a maximum, with no quantitative differences between the results pertaining suspensions with Giesekus and Oldroyd-B constitutive equations.

I. INTRODUCTION

Suspensions have been extensively studied over the last century due to their relevance in several processes, like, for example, those occurring in oil, cement, paper, and food industries[22]. Hence, there is a vast literature on suspension rheology, including theoretical, experimental, and numerical works. The rheological behavior of suspensions depends on the size, shape, and concentration of the suspended solid particles and on the rheology of the suspending liquid. Particle concentration is usually measured in terms of the volume fraction of the solid fillers, ϕ, the suspension being said 'dilute' for $\phi \leq 0.05$, 'semi-dilute' for $0.05 \leq \phi \leq 0.1$, and 'concentrated' for $\phi > 0.1$. Concentrated suspensions are the most interesting from the applicative point of view[3]. Concerning the suspending liquid, suspensions with Newtonian matrices have been receiving great attention since the seminal work by Einstein[10] (see, for example, the review by Tanner[29] and the references therein), yet suspensions of particles in non-Newtonian fluids play key roles in many technological fields, as energy (e.g., fracking fluids), material design (e.g., injected composite materials, pastes, and paints), and consumer product (e.g., liquid medicines and drugs)[28]. Many scientific papers dealing with the rheology of suspensions with non-Newtonian - especially viscoelastic - matrices are experimental, yet in the last

decade the problem has been tackled also from the computational point of view, in particular addressing the issue of shear-thickening under simple shear flow[18,19,31,33?] . The behavior of suspensions with non-Newtonian matrices has been discussed in several reviews[21,28,30]. In particular, the very recent contribution from Tanner[30] contains a survey on their response under oscillatory shear flow, which is often used in rheometry to determine the viscoelastic properties of complex fluids.

In the literature, inertia has been usually neglected in the determination of the storage modulus, G', and the loss modulus, G'', of suspensions subjected to oscillatory shear flow, yet it might come into play in some practical situations, for example when low-viscosity suspending liquids and/or high oscillatory frequencies are considered. If the system is modeled as inertialess, this could lead to misinterpretation of the measurements. Under certain conditions, even a pure Newtonian liquid can exhibit an apparent non-null G'-value[5,11,17]. The effects of inertia on the apparent viscoelastic moduli of suspensions of rigid spheres in a Newtonian matrix have been recently studied numerically by the authors[32].

In this paper, we study through immersed-boundary-method numerical simulations the effects of inertia on the storage and loss moduli of suspensions of mono-disperse non-colloidal rigid spheres in non-Newtonian liquids subjected to small amplitude oscillatory shear (SAOS) flow, from the dilute to the concentrated regime. To model the rheology of the suspending liquid, we consider the Carreau-Yasuda constitutive equation, yielding an inelastic shear-thinning behavior, the Giesekus constitutive

---
a)Electronic mail: massimiliano.villone@unina.it

equation, which predicts a shear-thinning viscoelastic behavior, and the Oldroyd-B constant-viscosity viscoelastic constitutive equation.

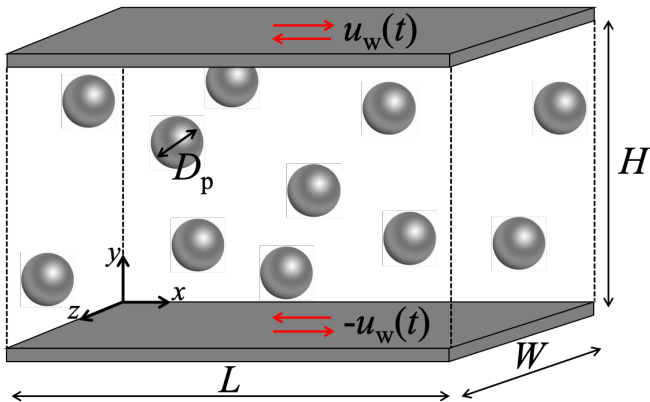## II. MATHEMATICAL MODEL AND NUMERICAL METHOD

FIG. 1: Schematic of a suspension of mono-disperse non-colloidal rigid spherical particles under oscillatory shear flow.

The system considered in our simulations is schematically represented in Fig. 1: a suspension of initially randomly distributed mono-disperse non-colloidal rigid spheres with diameter D_p undergoes SAOS flow in a plane Couette geometry, with x, y, and z denoting the streamwise, wall-normal, and spanwise directions. The moving walls of the flow cell are located at $y = 0$ and $y = H$, respectively, and move streamwise in opposite directions with oscillating velocity $u_\mathrm{w}(t) = (H/2)\gamma_0\omega\sin(\omega t)$, where γ_0 is the maximum deformation to which the system is subjected, ω is the oscillatory frequency, and t is the time. The geometrical confinement of the particles is measured by the blockage ratio D_p/H, which is equal to 0.2 for all the simulations reported in this paper, following previous studies[2,23,25,27,32]. This value is such that confinement effects on the measured suspension moduli are negligible, as it is shown in Fig. 17 by comparison with results at lower values of the blockage ratio. The dimensions of the flow cell in the streamwise and spanwise directions are $L = W = 8D_\mathrm{p}$. The system is considered to be periodic along these directions.

Assuming that gravity is negligible and that the suspending liquid is incompressible, its motion is governed by the mass and momentum balance equations, reading

$$\boldsymbol{\nabla} \cdot \boldsymbol{u} = 0, \tag{1}$$

$$\rho \left(\frac{\partial \boldsymbol{u}}{\partial t} + \boldsymbol{u} \cdot \boldsymbol{\nabla} \boldsymbol{u} \right) = \boldsymbol{\nabla} \cdot \boldsymbol{T} + \boldsymbol{f}, \tag{2}$$

with ρ the density of the liquid, $\boldsymbol{u}$ its velocity, $\boldsymbol{T}$ the Cauchy stress tensor, and $\boldsymbol{f}$ a body force used to account for the presence of the particles.

According to the inelastic shear-thinning Carreau-Yasuda constitutive equation, the stress tensor $\boldsymbol{T}$ can be expressed as[4]

$$\boldsymbol{T} = -p\boldsymbol{I} + 2\eta(\dot{\gamma})\boldsymbol{\mathcal{D}}, \tag{3}$$

with p the pressure, $\eta(\dot{\gamma})$ the dynamic viscosity of the liquid depending on the shear rate $\dot{\gamma} = \sqrt{2\boldsymbol{\mathcal{D}} : \boldsymbol{\mathcal{D}}}$, and $\boldsymbol{\mathcal{D}}$ the strain rate tensor defined as $\boldsymbol{\mathcal{D}} = (\boldsymbol{\nabla}\boldsymbol{u} + \boldsymbol{\nabla}\boldsymbol{u}^\mathrm{T})/2$. In particular, η depends on $\dot{\gamma}$ as

$$\eta(\dot{\gamma}) = \eta_\infty + (\eta_0 - \eta_\infty)[1 + (\tau\dot{\gamma})^a]^{\frac{n-1}{a}}, \tag{4}$$

with η_0 and η_∞ denoting the plateau levels to which the viscosity of the fluid tends at vanishing and diverging shear rate, respectively, τ the characteristic time, a and n model parameters. As said, the Carreau-Yasuda model predicts shear-thinning, namely, a decrease of the viscosity at increasing shear rate, with τ modulating the shear rate level above which the phenomenon occurs, corresponding to about $1/\tau$, and $a > 0$, $n \in]0, 1[$ describing the extent of the shear thinning. In this paper, we set $\eta_\infty/\eta_0 = 0.1$, $a = 2$, and $n = 0.3$.

Instead, when a viscoelastic liquid is considered, the stress tensor $\boldsymbol{T}$ reads

$$\boldsymbol{T} = -p\boldsymbol{I} + 2\eta_\mathrm{s}\boldsymbol{\mathcal{D}} + \boldsymbol{\sigma}, \tag{5}$$

where η_s is the 'solvent' contribution to the dynamic viscosity and $\boldsymbol{\sigma}$ is the viscoelastic extra-stress tensor, for which a constitutive equation has to be written. The Giesekus constitutive equation for $\boldsymbol{\sigma}$ reads[15]

$$\lambda\overset{\triangledown}{\boldsymbol{\sigma}} + \boldsymbol{\sigma} + \frac{\lambda\alpha}{\eta_\mathrm{p}}\boldsymbol{\sigma}^2 = 2\eta_\mathrm{p}\boldsymbol{\mathcal{D}}, \tag{6}$$

with λ the relaxation time, η_p the 'polymer' viscosity, α the so-called 'mobility parameter', and the symbol $\triangledown$ denoting the upper-convected time derivative[15]. The attributes 'solvent' and 'polymer' for the two contributions to the viscosity of a Giesekus fluid come from its typical use in modeling the rheological behavior of polymeric solutions. Notice that the zero-shear viscosity of a Giesekus liquid is $\eta_0 = \eta_\mathrm{s} + \eta_\mathrm{p}$. All the fluids considered in this paper have the same value of the zero-shear viscosity. The viscosity ratio of a Giesekus fluid, β, is defined as $\beta = \eta_\mathrm{s}/\eta_0$. The Giesekus model predicts shear-thinning, with the mobility parameter α modulating such effect: the larger α, the 'more' shear-thinning the fluid. On the other hand, when α goes to zero, the fluid has a constant viscosity and the Giesekus constitutive equation degenerates into the Oldroyd-B model[15]

$$\lambda\overset{\triangledown}{\boldsymbol{\sigma}} + \boldsymbol{\sigma} = 2\eta_\mathrm{p}\boldsymbol{\mathcal{D}}. \tag{7}$$

In Fig. 2, we report the predicted rheological behavior of the fluids considered in this paper when subjected to
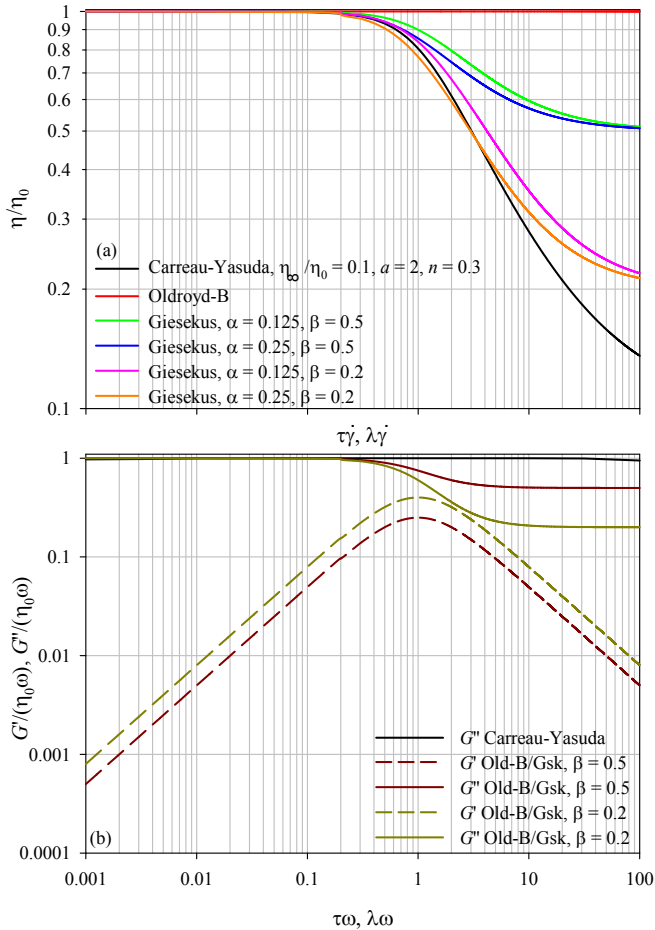
FIG. 2: Rheological behavior of the Carreau-Yasuda, Oldroyd-B, and Giesekus liquids considered in this paper when subjected to simple shear flow (a) and SAOS flow (b). The values of the constitutive parameters are given in the legend.

simple shear and SAOS flow in the absence of particles. From panel a, it is apparent that, given the values of the constitutive parameters indicated in the legend, the Carreau-Yasuda liquid undergoes shear-thinning when $\mathcal{O}(\tau\dot{\gamma}) > 10^{-1}$; on the other hand, its viscosity has not yet reached $\eta_\infty = 0.1\eta_0$ at $\tau\dot{\gamma} = 100$, i.e., the upper limit of the shear rate window displayed in the diagram. A qualitatively similar behavior is shown by the Giesekus fluid. For all the $\alpha - \beta$ couples considered here, shear thinning always arises when $\tau\dot{\gamma}$ is above 0.1 and it is enhanced at increasing α and decreasing β, as the viscosity plateau at high shear rate is equal to $\beta\eta_0$. Of course, the Oldroyd-B constitutive equation predicts a constant shear viscosity. In panel b, the linear viscoelastic properties of the fluids are reported. Being a generalized Newtonian fluid, the Carreau-Yasuda constitutive equation predicts zero storage modulus, whereas the loss modulus is substantially constant over the whole window of dimensionless

frequency, $\tau\omega$, shown in the graph. The loss modulus of a Giesekus liquid behaves analogously to its shear viscosity, namely, it exhibits thinning for $\mathcal{O}(\lambda\omega) > 10^{-1}$ until reaching the plateau value at high frequency equal to β times the value at vanishing ω. On the other hand, the storage modulus has a non-monotonic trend with $\lambda\omega$ and attains a maximum at $\lambda\omega = 1$. From the quantitative point of view, β has an opposite effect on the moduli, as decreasing β makes G' increase and G'' decrease. Finally, it is worth remarking that changing α has no effect at all on the storage and loss moduli of a Giesekus liquid (or an Oldroyd-B liquid, this being a Giesekus liquid with $\alpha = 0$).

The motion of the particles is governed by the Newton-Euler equations. With reference to the generic k-th particle, these read

$$\rho_\mathrm{p}\mathcal{V}_\mathrm{p}\frac{d\boldsymbol{u}_{\mathrm{p},k}}{dt} = \oint_{\partial P_k} \boldsymbol{T} \cdot \boldsymbol{n}_k \; dA + \boldsymbol{F}_k, \qquad (8\mathrm{a})$$

$$\mathcal{I}_\mathrm{p}\frac{d\boldsymbol{\omega}_{\mathrm{p},k}}{dt} = \oint_{\partial P_k} \boldsymbol{r}_k \times (\boldsymbol{T} \cdot \boldsymbol{n}_k) \; dA + \boldsymbol{T}_k, \qquad (8\mathrm{b})$$

where $\boldsymbol{u}_{\mathrm{p},k}$ is the particle centroid velocity, $\boldsymbol{\omega}_{\mathrm{p},k}$ is the particle angular velocity, ∂P_k identifies the particle boundary, dA is a differential surface area element, and ρ_p, $\mathcal{I}_\mathrm{p}$, and $\mathcal{V}_\mathrm{p}$ are the particle density, moment of inertia, and volume, respectively. In particular, for a rigid sphere with radius r_p, one gets $\mathcal{V}_\mathrm{p} = (4/3)\,\pi r_\mathrm{p}^3$ and $\mathcal{I}_\mathrm{p} = (2/5)\,\rho_\mathrm{p}\mathcal{V}_\mathrm{p}r_\mathrm{p}^2$. Moreover, $\boldsymbol{r}_k$ is the position vector relative to the particle centroid, $\boldsymbol{n}_k$ is the unit normal vector pointing outwards from the particle, and $\boldsymbol{F}_k$ and $\boldsymbol{T}_k$ are the force and torque acting on the particle due to particle-particle and particle-wall interactions. The density ratio of the suspension ρ_p/ρ is considered equal to 1, i.e., the particles are neutrally buoyant.

The balance equations reported above are supplied with appropriate boundary conditions: a velocity $-u_\mathrm{w}(t)$ is assigned to the channel sliding wall at $y = 0$ and a velocity $u_\mathrm{w}(t)$ is assigned to the channel sliding wall at $y = H$, the periodicity of fluid velocity and stress is prescribed on the flow cell faces at $x = 0$ and $x = L$ and at $z = 0$ and $z = W$, respectively, and the no-slip/no-penetration conditions are imposed on the particle boundaries. At the initial time, the fluid is considered still and stress-free and laden with randomly distributed still particles. The initial random spatial distribution of the particles is the same given the values of the confinement ratio and of the volume fraction of the solid phase.

The time integration of the equations is based on an explicit fractional-step method[14], where all the terms are advanced with the third order Runge-Kutta scheme. The governing differential equations are solved on a staggered grid using a second-order central finite-difference scheme. In order to couple the motion of the fluid and the particles, we employ the immersed boundary method (IBM) proposed by Breugem[6] and based on the direct-forcing approach, which has been used in several previous studies on rigid particle suspensions[1,2,23,24,26]. Such IBM is

second-order accurate. Lubrication interactions are automatically included in our code, yet, when the distance between two particles is smaller than one Eulerian grid cell, the lubrication force is under-predicted by the IBM due to the finite grid size. To compensate for this inaccuracy and to avoid computationally expensive grid refinements, a lubrication correction model based on the asymptotic analytical expression for the normal lubrication force between spheres in a Newtonian fluid is used[7]. Such model proved effective also for suspensions with non-negligible inertia. In addition, a soft-sphere collision model with Coulomb friction takes over the interaction when the particles touch. The restitution coefficients used for normal and tangential collisions are 0.97 and 0.1, respectively, with the Coulomb friction coefficient set to 0.15. It is worth remarking that, even if a Newtonian lubrication model is used, the contact model influences the results much more than the lubrication model and it does not depend on the fluid rheology for $\phi \lesssim 0.3$[7,12]. Also, due to the small displacements considered in this work, the particles do not touch. A complete description of the numerical scheme and a validation campaign are reported by Izbassarov and co-authors[13]. In this paper, mesh convergence is achieved with elements with a size of $3.125 \times 10^{-2} r_{\mathrm{p}}$, thus the Eulerian grid is composed by about 10.5×10^6 elements, whereas the surface of each particle is resolved through 3219 Lagrangian points, i.e., 32 points per particle diameter. Time discretization depends on the flow characteristic time. In this work, timesteps ranging from $\mathcal{O}(10^{-6}/\omega)$ to $\mathcal{O}(10^{-2}/\omega)$ are used, yielding computational times between a few hours (for the cases at largest inertia) to a couple of months (for the cases at lowest inertia).

III. RESULTS

For both the inelastic and the elastic matrices, two dimensionless numbers can be defined, namely, the Stokes number, $\mathrm{St} = \rho H^2 \omega / \eta_0$, measuring the relative importance of inertial and viscous effects, and the ratio of the fluid and the process characteristic times. For the Carreau-Yasuda liquid, this is given by the Carreau number, $\mathrm{Cu} = \tau \omega$, whereas, when a viscoelastic liquid is considered, we introduce the Deborah number, $\mathrm{De} = \lambda \omega$. In this paper, we consider $\mathrm{St}^{1/2}$ ranging between 1.0 and 50, Cu between 0.1 and 100, and De between 0.1 and 2.0. Experimental results obtained from systems characterized by the same values of the dimensionless parameters as those considered in the simulations could be compared with the numerical results. Just to make an example, a suspension of particles with a diameter of 200 μm in a fluid with density of 1000 kg m^{-3} and viscosity of 0.001 Pa × s oscillating at a frequency of 15 s^{-1} in a rheometer with a gap of 1 mm is characterized by $\mathrm{St}^{1/2} = 3.87$. Another way of evaluating the relative importance of inertial and viscous effects is, of course, to compute the flow and particle Reynolds num-

bers, which are combinations of the other, independent, dimensionless parameters. In particular, the flow Reynolds number can be expressed as $\mathrm{Re} = \rho u_{\mathrm{w,max}} H / \eta_0 = \rho(\gamma_0 \omega H/2) H / \eta_0 = (\gamma_0/2)\mathrm{St}$, thus it ranges from 0.0025 to 6.25, whereas the particle Reynolds number can be expressed as $\mathrm{Re_p} = \rho(\gamma_0 \omega H/2) r_{\mathrm{p}} / \eta_0 = (\gamma_0/4)(D_{\mathrm{p}}/H)\mathrm{St}$, thus it ranges from 0.00025 to 0.625.

In a suspension undergoing SAOS flow with amplitude γ_0 and frequency ω, the shear stress can be expressed as[16]

$$T_{\mathrm{xy}}(t) = \gamma_0(G'\cos(\omega t) + G''\sin(\omega t)), \qquad (9)$$

where G' and G'' are the storage and loss moduli of the system, respectively. When SAOS flow conditions hold, there is a linear relationship between the imposed strain and the measured stress, namely,

$$\frac{T_{\mathrm{xy}}(t)|_{2\gamma_0}}{2\gamma_0} = \frac{T_{\mathrm{xy}}(t)|_{\gamma_0}}{\gamma_0}. \qquad (10)$$

Consequently, one gets $(G', G'')|_{2\gamma_0} = (G', G'')|_{\gamma_0}$. We verify that the aforementioned condition is fulfilled for $\gamma_0 = 0.005$, thus the numerical results presented below refer to such value.
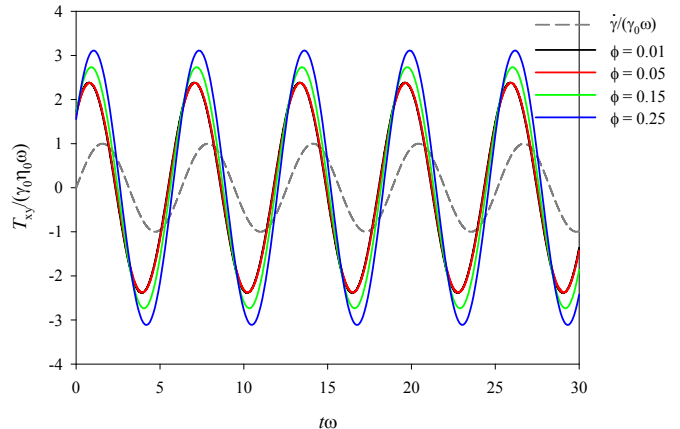
A. Carreau-Yasuda inelastic suspending liquid

FIG. 3: Dynamics of the shear stress in a suspension of mono-disperse non-colloidal rigid spheres in a Carreau-Yasuda liquid subjected to SAOS flow at $\mathrm{St}^{1/2} = 5.0$ and $\mathrm{Cu} = 0.5$ for 4 different values of the volume fraction, ϕ, as indicated in the legend. The gray dashed line gives the dimensionless applied shear rate $\dot{\gamma}/(\gamma_0 \omega)$.

In Fig. 3, we report the temporal history of the shear stress in a suspension of mono-disperse non-colloidal rigid spheres in a Carreau-Yasuda liquid subjected to SAOS flow at $\mathrm{St}^{1/2} = 5.0$ and $\mathrm{Cu} = 0.5$ for four values of the volume fraction of the solid phase from the dilute to the

concentrated regime, namely, $\phi = 0.01, 0.05, 0.15, 0.25$. On the horizontal axis, the time is made dimensionless with the oscillatory frequency, ω, whereas, on the vertical axis, the shear stress is normalized by the 'Newtonian' maximum stress, $\gamma_0 \eta_0 \omega$. It can be seen that the shear stress undergoes periodic oscillations, that the maximum (respectively, the minimum) stress level increases (respectively, decreases) at increasing ϕ, and that the stress curves corresponding to the different values of the volume fraction are not synchronous; indeed, the greater ϕ the more the stress curve 'lags' with respect to the applied forcing wave, as it can be observed by looking at the gray dashed line representing the dimensionless applied shear rate, $\dot{\gamma}/(\gamma_0 \omega)$. The increased delay at larger volume fractions had been already observed for suspensions with Newtonian matrices at non-negligible inertia[32].

We perform a linear least squares regression of stress data like those displayed in Fig. 3 based on Eq. (9), so obtaining the values of the viscoelastic moduli at varying St and Cu reported in Fig. 4, where the lines connecting the computed data have the scope of guiding the eye.

On the left, the dimensionless storage modulus of the suspension, $G'/(\eta_0 \omega)$, is plotted as a function of the Carreau number, Cu, for the different values of the particle volume fraction, ϕ, under investigation. Each row pertains a different value of the square root of the Stokes number, $\mathrm{St}^{1/2}$. Notice that the data at $\mathrm{Cu} = 0.001$ actually correspond to simulations with a Newtonian suspending liquid, but, since the Cu-scale is logarithmic, they are conventionally attributed to such Cu for visualization purposes. Several remarks can be made. First of all, like in suspensions with a Newtonian matrix[32], it holds true that, when inertia is non-negligible, i.e., St is not zero, the oscillatory measurement 'reads' a non-null value of the storage modulus, thus inertia acts as an apparent elasticity. Fixed Cu and ϕ, G' increases by orders of magnitude with St, as it can be observed by looking at the values on the vertical axis in each panel. On the other hand, G' only moderately changes with the concentration of the solid phase, yet the direction of its variation is non-monotonic. Indeed, G' slightly decreases with ϕ at every Cu for $\mathrm{St}^{1/2} = 1.0$, 5.0, and 50 (see panels a1, b1, and d1), whereas it increases with ϕ at $\mathrm{St}^{1/2} = 10$, except at $\mathrm{Cu} = 100$, where the decreasing trend is recovered (see panel c1). Such unusual behavior had been already observed in suspensions with a Newtonian matrix (see the values at $\mathrm{Cu} \to 0$ and Fig. 4a in Villone et al.[32]) and may require further investigation (even experimentally). Finally, increasing Cu has essentially no effect on G' at $\mathrm{St}^{1/2} = 1.0$, whereas, at larger St, no effect is seen for Cu below 1. As the order of magnitude of Cu further increases to 10 and 100, a significant decrease of the suspension storage modulus occurs, which is progressively more pronounced at increasing St. This might appear somehow counterintuitive. Indeed, given the oscillatory frequency, ω, Cu can be increased by increasing the liquid characteristic time, τ, which, in turn, corresponds to a decrease of the characteristic value of the shear rate above

which the suspending liquid undergoes shear-thinning: as the shear rate oscillates between zero and its maximum, $\gamma_0 \omega$, the greater Cu the larger the time in which the system overcomes the threshold for the occurrence of shear-thinning, thus it should 'feel' a larger St than the applied value (whose definition is based on the zero-shear viscosity). This would suggest an increase of G' with Cu, yet it is observed that increasing Cu above $\mathcal{O}(10)$ hinders the apparent elasticity of the suspension.

The behavior of the dimensionless loss modulus of the suspension, $G''/(\eta_0 \omega)$, is displayed on the right column of Fig. 4. Given Cu and ϕ, G'' significantly increases with St (compare the values on the vertical axis among the four panels). In addition, also the concentration of the solid fillers has an appreciable effect on the loss modulus that always increases with ϕ, even if such effect is progressively less relevant at increasing St and Cu. (For example, at $\mathrm{St}^{1/2} = 50$ and $\mathrm{Cu} = 100$, the values of the loss modulus corresponding to the different particle concentrations collapse.) Finally, at fixed $\mathrm{St}^{1/2}$ and ϕ, there are no deviations of the loss moduli of suspensions with a Carreau-Yasuda matrix from those of suspensions with a Newtonian matrix for Cu below $\mathcal{O}(1)$, whereas a significant decrease of G'' occurs when Cu is above $\mathcal{O}(10)$ that is progressively more pronounced at increasing St. The decrease of the loss modulus at high Cu might be explained by considering that the greater Cu the longer the time the system undergoes shear-thinning, which leads to a decrease of the loss modulus.

In Fig. 5, the dimensionless storage and loss moduli of the suspension are plotted against $\mathrm{St}^{1/2}$ at $\mathrm{Cu} = 0.1$ (top) and 100 (bottom) for $\phi = 0.01$ and 0.25. At low Cu, an analogous behavior to that observed for suspensions with a Newtonian matrix[32] is seen: when the particle concentration is low, G'' dominates on G' at low St, then G' overlaps G'' for $\mathrm{St}^{1/2} \gtrsim 5.0$, whereas, when the suspension is concentrated, G' stays always below G'', yet their distance progressively decrease and they overlap around $\mathrm{St}^{1/2} = 50$. At high Cu and low ϕ, the behavior is analogous to that at low ϕ and low Cu, whereas no overlap between the storage and the loss modulus is observed at high particle concentration: at low St, G'' dominates on G', then, at increasing St, the curves representing these two quantities become almost parallel.

In order to deepen the interpretation of the results reported above, we display in Fig. 6 the spatial distribution of the particles in a suspension with $\phi = 0.15$ for four $\mathrm{St}^{1/2} - \mathrm{Cu}$ combinations. On the top row, we also display the color maps of the fluid dimensionless streamwise velocity on the flow cell moving walls, the xy-plane at $z = 0$, and the yz-plane at $x = 0$ at $t\omega = 5\pi/2$. These show that at moderate $\mathrm{St}^{1/2} = 5.0$ (first two snapshots on the row), the streamwise velocity profile recalls the linear velocity profile that would characterize an inertialess pure liquid, yet it is perturbed (see below) due to non-negligible inertia and to the presence of the particles, as it is apparent by looking at the map on the yz-plane at $x = 0$. When Cu
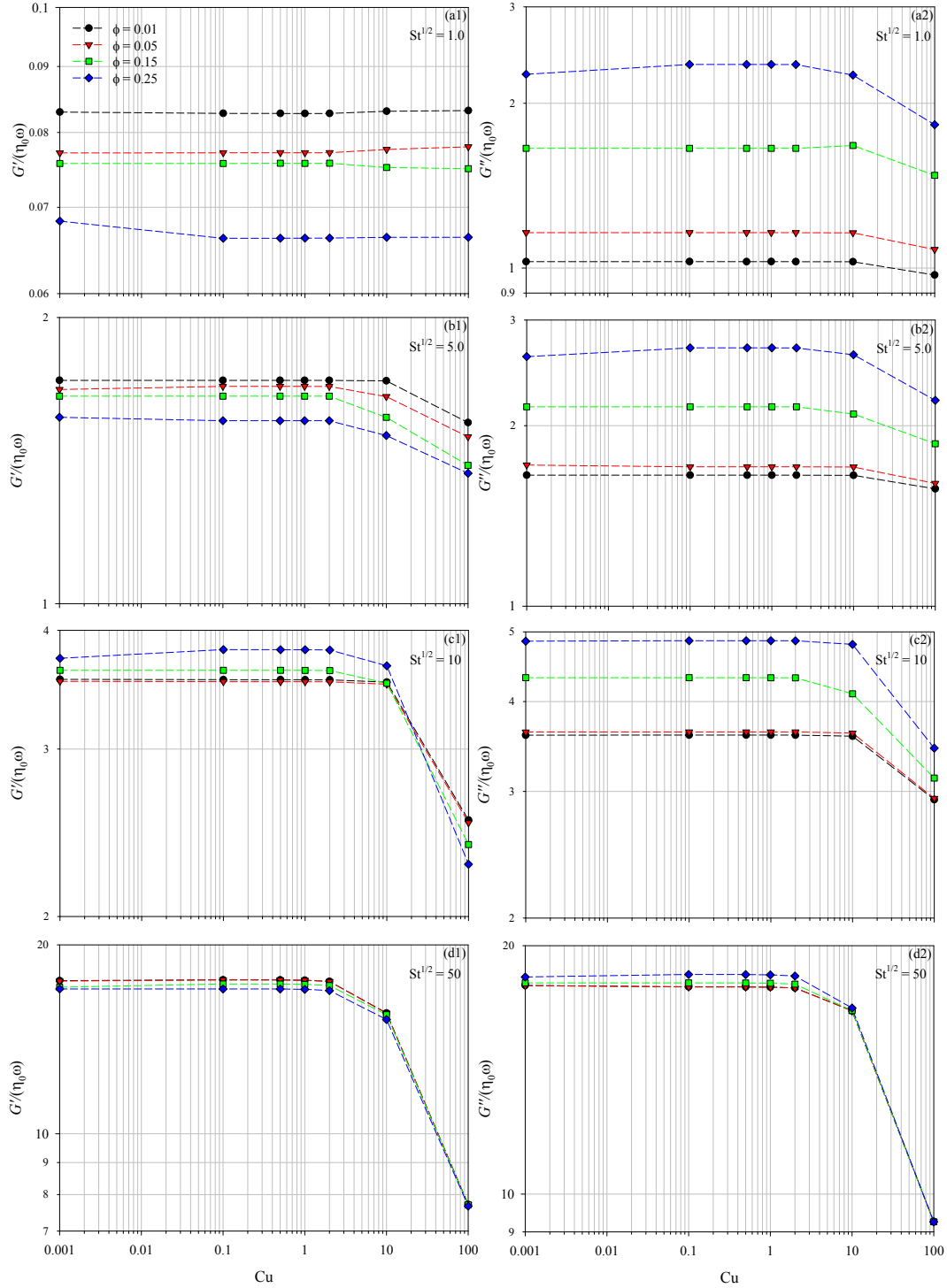
FIG. 4: Dimensionless storage modulus $G'/(\eta_0\omega)$ (left column) and loss modulus $G''/(\eta_0\omega)$ (right column) as a function of the Carreau number, Cu, for a suspension of mono-disperse non-colloidal rigid spheres in a Carreau-Yasuda liquid subjected to SAOS flow. The data pertain the different values of the particle volume fraction, ϕ, indicated in the legend. Each row corresponds to a different value of the square root of the Stokes number, $St^{1/2}$, as indicated in the panels. The lines connecting the data have the scope of guiding the eye. The data at Cu = 0.001 correspond to a Newtonian suspending liquid and are conventionally attributed to such Cu for visualization purposes.

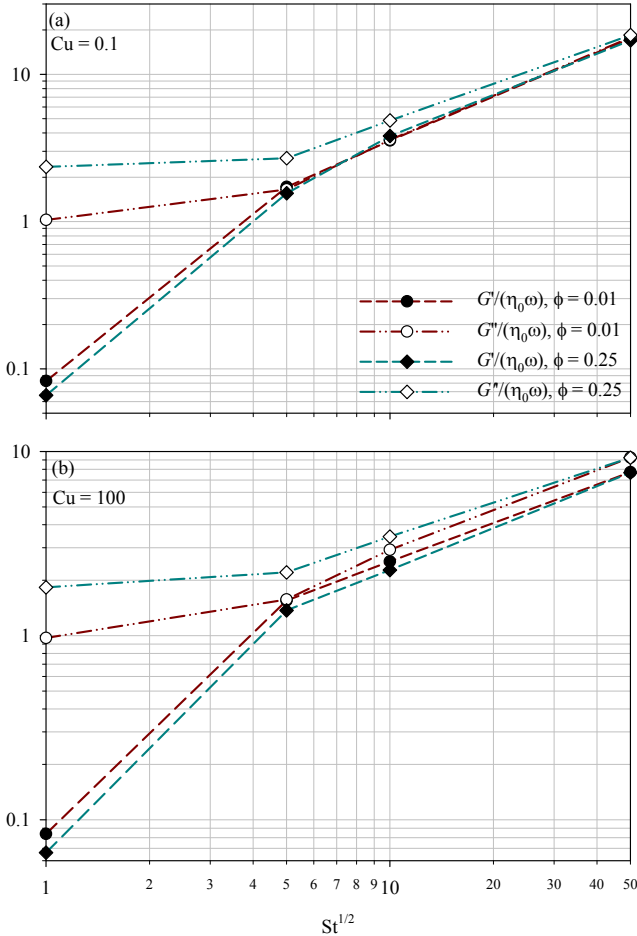is changed, no qualitative effects on the fluid streamwise velocity are observed. On the bottom row, the color maps

FIG. 5: Dimensionless storage modulus, $G'/(\eta_0\omega)$, and loss modulus, $G''/(\eta_0\omega)$, as a function of $St^{1/2}$ for a suspension of mono-disperse non-colloidal rigid spheres in a Carreau-Yasuda liquid subjected to SAOS flow at $Cu = 0.1$ (a) and 100 (b). Two values of the particle volume fraction, ϕ, are considered, as indicated in the legend. The lines connecting the data have the scope of guiding the eye.

of the fluid dimensionless wall-normal velocity show that at $St^{1/2} = 5.0$ (first two snapshots), the particles induce the appearance of wall-normal components in the fluid velocity within 4% of the maximum streamwise velocity. No significant effects are observed neither on the fluid wall-normal velocity when Cu is changed. On the other hand, at high $St^{1/2} = 50$, the fluid streamwise velocity field is way different from the inertialess case. As it is shown by the third and fourth top images, close to both the upper and the lower wall of the flow cell, the velocity goes from the wall value to almost zero in a thin layer (with a height of about $0.1H$), whereas a thick region in between the walls is practically still. This explains the increase of the shear stress levels, and thus of the suspension

moduli, at increasing St; indeed, since the velocity drops from the maximum value to zero over a small distance, the actual shear rate in the thin layers close to the walls is much larger than the overall imposed value, leading to an enhancement of the shear stress at the walls. In other words, the actual deformation to which the system is subjected in such layers is about 10 times the 'global' deformation. In addition, the observation that at high St the fluid has a vanishing velocity in a large part of the channel gap can help to explain why the effects of particle concentration are almost negligible when inertia is very relevant. On the bottom row, the last two color maps show that, at $St^{1/2} = 50$, the wall-normal components of the fluid velocity are much lower than at $St^{1/2} = 5.0$, with a further reduction at increasing Cu.

A more quantitative description of such observations is given in Fig. 7a, where we display the vertical profiles of the xz-surface average of the fluid dimensionless streamwise velocity corresponding to the four snapshots given in Fig. 6. We also report through a gray dashed line the linear velocity profile characteristic of a pure inertialess liquid, from which the profiles at non-negligible inertia are seen to detach. At $St^{1/2} = 5.0$, the streamwise velocity profiles get curved and show an inflection point around the midplane of the flow cell. A quantitative effect is observed when Cu is increased, since there is an increase of the curvature of the two parts of the profile, below and above the inflection point. On the other hand, a flattening of the streamwise velocity profiles occurs at $St^{1/2} = 50$, where the velocity drops from the wall value to zero over a thin distance, which becomes even thinner at increasing Cu. In Fig. 7b, we report the profiles of the fluid dimensionless streamwise velocity at $Cu = 0.1$ and $St^{1/2} = 5.0, 50$ for $t\omega = 5\pi/2, 3\pi, 7\pi/2$, namely, when the upper wall has the maximum positive velocity, when the walls invert their movement, and when the upper wall has the maximum negative velocity. The three profiles at $St^{1/2} = 5.0$ are all curved with an inflection point at the channel midplane, where the velocity is always null. In particular, it can be observed that, at $t\omega = 3\pi$, the velocity of the walls vanishes, yet the fluid along the channel gap still keeps moving due to inertia. On the other hand, at $St^{1/2} = 50$, the fluid flow induced by the walls' oscillatory movement is confined in the aforementioned layers close to the walls, whereas the central region of the channel in the wall-normal direction keeps substantially still.

It is known from the literature that inertia might induce cross-streamline migration of rigid particles in sheared liquids[20], thus altering the random distribution of the particles in the flow cell by deterministically 'pushing' them towards two equilibrium horizontal planes, and consequently influencing the shear stress in the suspension. However, due to the very modest amplitude of the oscillations, lateral migration does not play any role over the observation time in the cases considered here, neither at the largest St. As an illustrative example, we show in Fig.
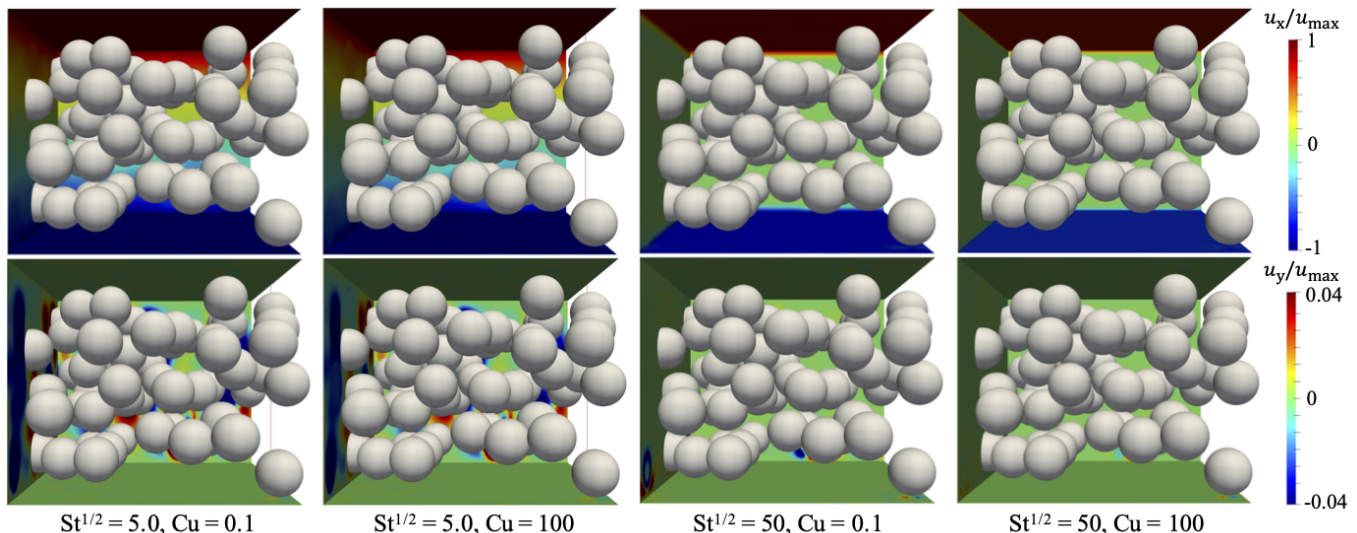
FIG. 6: Particle distribution and maps of the fluid dimensionless streamwise (top) and wall-normal (bottom) component on the moving walls, the xy-plane at $z = 0$, and the yz-plane at $x = 0$ for a suspension of mono-disperse non-colloidal rigid spheres in a Carreau-Yasuda liquid with $\phi = 0.15$ subjected to SAOS flow. Four $\mathrm{St}^{1/2} - \mathrm{Cu}$ combinations are considered. The snapshots refer to $t\omega = 5\pi/2$ and the velocity-values are normalized by the maximum oscillatory velocity of the walls, $u_{\mathrm{max}} = (H/2)\gamma_0\omega$.

8 the temporal evolution of the vertical positions of all the particles in the flow cell normalized over the available space along the channel gap, $(y_{\mathrm{p}} - r_{\mathrm{p}})/(H(1 - D_{\mathrm{p}}/H))$, in a suspension with $\phi = 0.15$ oscillating at $\mathrm{St}^{1/2} = 50$ and $\mathrm{Cu} = 100$. None of the particles in the flow cell has a detectable displacement in the wall-normal direction.

B. Viscoelastic suspending liquids

In this section, we investigate the SAOS flow of suspensions with viscoelastic matrices. In particular, we first report on the effects of the variation of the Stokes and Deborah numbers on the measured storage and loss moduli of suspensions of mono-disperse non-colloidal rigid spheres in a Giesekus fluid with mobility parameter $\alpha = 0.125$ and viscosity ratio $\beta = 0.5$.

In Fig. 9, we show the dynamics of the shear stress in a suspension subjected to SAOS flow at $\mathrm{St}^{1/2} = 10$ and $\mathrm{De} = 1.0$ for the same four values of the particle volume fraction considered above, i.e., $\phi = 0.01, 0.05, 0.15, 0.25$. As in Fig. 3, the time is made dimensionless by multiplication with the oscillatory frequency, ω, and the shear stress is normalized by the 'Newtonian' maximum stress, $\gamma_0\eta_0\omega$. It is apparent that each stress curve undergoes a brief transient, before reaching a periodic regime. The vertical gray dashed line marks a dimensionless time equal to 4π, which is the time the moving walls take to perform two oscillatory cycles. Such time is here observed to be sufficient for each stress curve to reach the periodic regime: we, therefore, perform regression of the stress data through Eq. (9) starting from the stress value at

$t\omega = 4\pi$.

The regression of the stress temporal history at varying St and De yields the viscoelastic moduli reported in Fig. 10, where the lines connecting the computed data have the scope of guiding the eye.

On the left column, the dimensionless storage modulus of the suspension, $G'/(\eta_0\omega)$, is plotted as a function of the Deborah number, De, for the different values of the particle volume fraction, ϕ, under investigation. Each row corresponds to a different value of the square root of the Stokes number, $\mathrm{St}^{1/2}$. We also point out that the data at $\mathrm{De} = 0.001$ actually pertain simulations with a Newtonian suspending liquid, yet, since the De-scale is logarithmic, they are conventionally attributed to such De for visualization purposes. By comparing the panels along the column, it can be remarked that, given De and ϕ, the storage modulus increases by orders of magnitude with St as an effect of the increasing apparent elasticity provided by inertia[32]. On the other hand, given St and ϕ, G' always attains a maximum at $\mathrm{De} = 0.1$ (except at $\mathrm{St}^{1/2} = 1.0$, $\phi = 0.25$) and then decreases with De. This qualitatively reproduces the behavior of an inertialess Giesekus liquid, yet with an important quantitative difference: indeed, at given oscillatory frequency, the storage modulus of the pure liquid increases at low De, it attains a maximum at $\mathrm{De} = 1$, then decreases further increasing De, as displayed in Fig. 2b . Finally, it can be observed that G' only moderately changes with the concentration of the solid phase, though the direction of such variation is non-monotonic. In fact, G' decreases with ϕ at $\mathrm{St}^{1/2} = 1.0$ and 1.0 (see panels a1 and c1), whereas it increases with ϕ at $\mathrm{St}^{1/2} = 5.0$ (see panel b1). On the other hand,

FIG. 8: Temporal evolution of the normalized vertical positions of the particles in a suspension of mono-disperse non-colloidal rigid spheres in a Carreau-Yasuda liquid with $\phi = 0.15$ subjected to SAOS flow at $St^{1/2} = 50$ and Cu = 100.
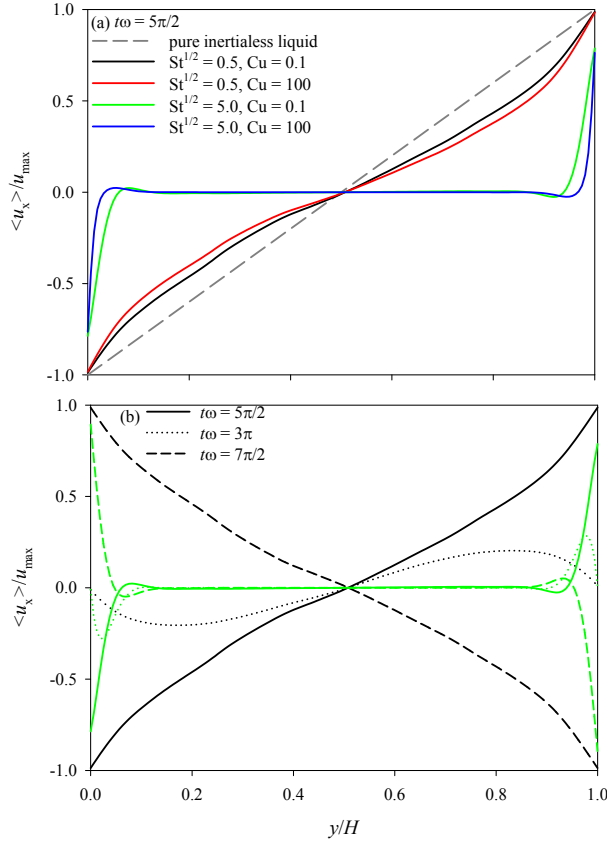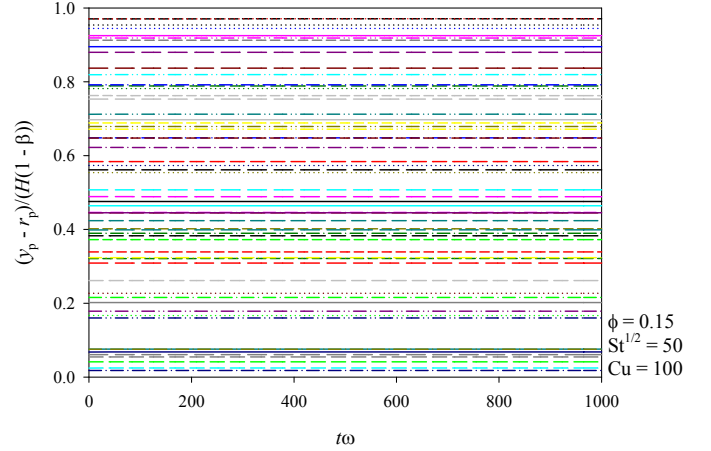

FIG. 7: Vertical profiles of the xz-surface average of the fluid dimensionless streamwise velocity in a suspension of mono-disperse non-colloidal rigid spheres in a Carreau-Yasuda liquid with $\phi = 0.15$ subjected to SAOS flow. The velocity-values are normalized by the maximum oscillatory velocity of the walls, $u_{\max} = (H/2)\gamma_0\omega$. In panel a, four $St^{1/2} - $ Cu combinations are considered, as indicated in the legend, and the profiles refer to $t\omega = 5\pi/2$; in panel b, two $St^{1/2} - $ Cu couples are considered and the profiles refer to $t\omega = 5\pi/2, 3\pi, 7\pi/2$.
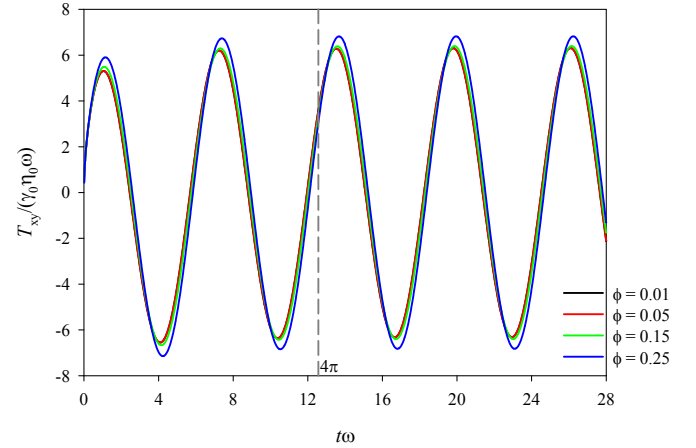

FIG. 9: Dynamics of the shear stress in a suspension of mono-disperse non-colloidal rigid spheres in a Giesekus liquid with $\alpha = 0.125$ and $\beta = 0.5$ subjected to SAOS flow at $St^{1/2} = 10$ and De = 1.0 for 4 different values of the volume fraction, ϕ, as indicated in the legend.

there is substantially no dependence of the suspension storage modulus on the filler volume fraction at high St: it is apparent from panel d1 that the points at different ϕ collapse when $St^{1/2} = 50$.

The data pertaining to $G''/(\eta_0\omega)$ are shown on the right column of Fig. 10, following the same layout as for $G'/(\eta_0\omega)$ on the left. Given De and ϕ, G'' increases with St (compare the values on the vertical axis among the four panels), but its quantitative variation is weaker than the one experienced by G'. At low $St^{1/2} = 1.0$ (see panel a2), fixed ϕ, the loss modulus monotonically decreases with De, which is consistent with the known literature results referring to the inertialess case[8], whereas a maximum is found at De $\simeq 0.5$ for larger values of the Stokes number. Concerning the concentration of the particles, the loss

modulus of the suspension always increases with ϕ except at $St^{1/2} = 50$, where the values of G'' at different ϕ collapse (see panel d2).

In Fig. 11, the dimensionless storage and loss moduli of the suspension are plotted against $St^{1/2}$ for $\phi = 0.01$ and 0.25 at De = 0.1 (top) and 2.0 (bottom). At low De, an analogous behavior to that observed for suspensions with a Newtonian matrix[32] is seen: at low $St^{1/2}$, the loss modulus always dominates over the storage modulus, then, when the suspension is dilute, G' overlaps G'' for
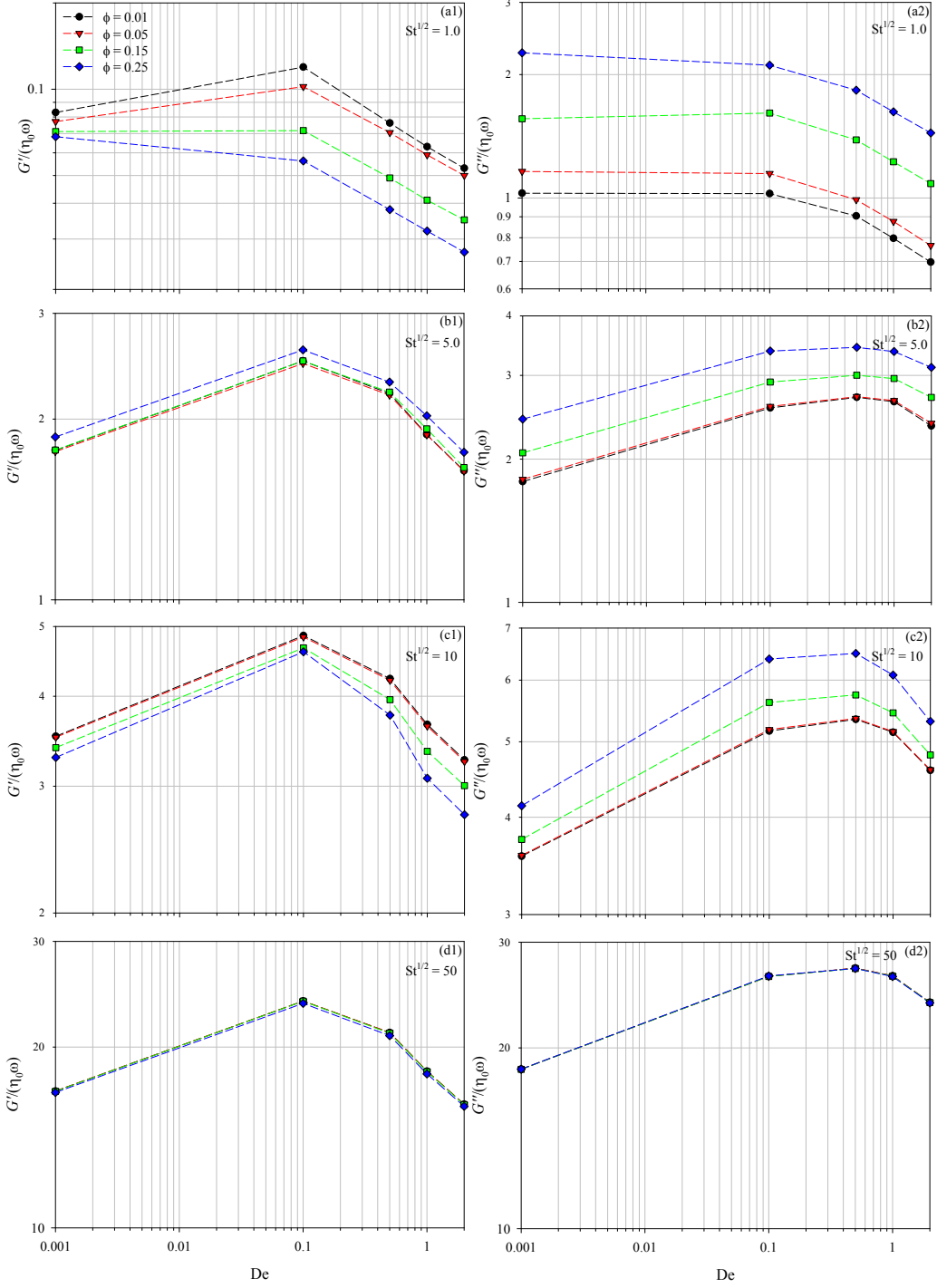
FIG. 10: Dimensionless storage modulus $G'/(\eta_0\omega)$ (left column) and loss modulus $G''/(\eta_0\omega)$ (right column) as a function of the Deborah number, De, for a suspension of mono-disperse non-colloidal rigid spheres in a Giesekus liquid with $\alpha = 0.125$ and $\beta = 0.5$ subjected to SAOS flow. The data pertain the different values of the particle volume fraction, ϕ, indicated in the legend. Each row corresponds to a different value of the square root of the Stokes number, $St^{1/2}$, as indicated in the panels. The lines connecting the data have the scope of guiding the eye. The data at De = 0.001 correspond to a Newtonian suspending liquid and are conventionally attributed to such De for visualization purposes.

$St^{1/2} \gtrsim 5$, whereas, when the system is concentrated, G'' always stays above G' and the two trends are almost
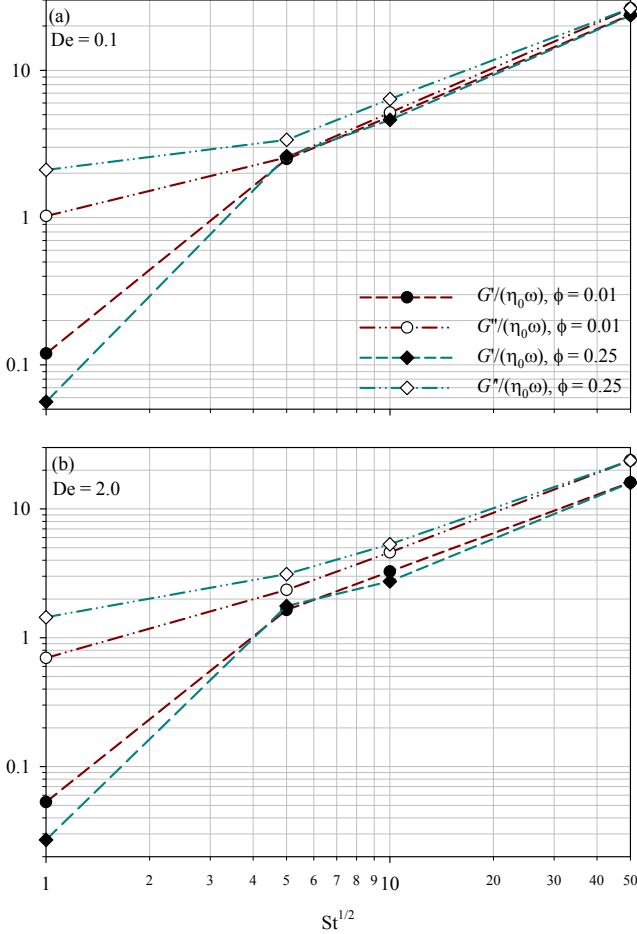
FIG. 11: Dimensionless storage modulus, $G'/(\eta_0\omega)$, and loss modulus, $G''/(\eta_0\omega)$, as a function of $\mathrm{St}^{1/2}$ for a suspension of mono-disperse non-colloidal rigid spheres in a Giesekus liquid with $\alpha = 0.125$ and $\beta = 0.5$ subjected to SAOS flow at De = 0.1 (a) and 2.0 (b). Two values of the particle volume fraction, ϕ, are considered, as indicated in the legend. The lines connecting the data have the scope of guiding the eye.

parallel for $\mathrm{St}^{1/2} \gtrsim 5$. The latter scenario holds true at high De regardless of ϕ (see panel b).

In order to deepen the comprehension of the results reported above, it might be useful to visualize separately the solvent and polymer contributions to the suspension shear stress, i.e., those arising from the second and the third term of the rhs of Eq. (5). This is done in Fig. 12 for four combinations of St and De and for the lowest and the highest particle volume fraction, namely, $\phi = 0.01$ and 0.25. By comparing the behaviors at low $\mathrm{St}^{1/2} = 5.0$ (top row) and high $\mathrm{St}^{1/2} = 50$ (bottom row), two main remarks can be made: first, the order of magnitude of the stress contributions increases at increasing St, which reflects on the corresponding increase of the order of magnitude

of the moduli; in addition, quantitative differences are detected at low St between the curves at different particle concentration, whereas these overlap at high St, which results in the collapse of the G'- and G''- data at different ϕ observed at large St. On the other hand, by comparing the curves at low De = 0.1 and high De = 2.0 (right column), the same behavior of the phase shift between the solvent and the polymer stress contributions can be observed regardless of St: at low De, these are almost in phase, becoming instead almost in opposite phase at high De. The persistence of such behavior at varying St corresponds to the qualitative similarity among the plots of G' and G'' as function of De at different St.

As a further element of analysis, we display in Fig. 13 the spatial distribution of the particles in a suspension with $\phi = 0.15$ and the color maps of the fluid dimensionless streamwise (top) and wall-normal (bottom) velocity at $t\omega = 5\pi/2$ for four $\mathrm{St}^{1/2} - \mathrm{De}$ combinations. Similar considerations as those on Fig. 6 can be made, with De here playing the role there played by Cu. At low $\mathrm{St}^{1/2} = 5.0$, the streamwise velocity profile qualitatively looks like that of an inertialess pure liquid, yet perturbed due to non-negligible inertia and to the presence of the particles, with no significant changes at increasing De. As above, the particles induce wall-normal components of the fluid velocity within 4% of the maximum streamwise velocity. At increasing De, no significant effects are observed on the fluid wall-normal velocity. At high $\mathrm{St}^{1/2} = 50$, the fluid streamwise velocity field is such that it goes from the wall value to almost zero in a thin layer, whereas a thick region in between the walls is practically still, as already observed for the Carreau-Yasuda matrix; this explains the observed increase of the shear stress levels, thus of the suspension moduli, at increasing St. As above, the wall-normal components of the fluid velocity are much lower at $\mathrm{St}^{1/2} = 50$ than at $\mathrm{St}^{1/2} = 5.0$, with no significant variations at increasing De.

In Fig. 14, we report the vertical profiles of the xz-surface average of the fluid dimensionless streamwise velocity corresponding to the four snapshots in Fig. 13. Again, similar considerations as those on Fig. 7 can be made. At $\mathrm{St}^{1/2} = 5.0$, the streamwise velocity profiles get curved and show an inflection point at about $y/H = 0.5$, thus departing from the linear velocity profile for a pure inertialess Giesekus fluid (see gray dashed line). When De is increased, the curvature of the profile correspondingly increases. Instead, at $\mathrm{St}^{1/2} = 50$, there is a flattening of the streamwise velocity profiles that go from the wall value to zero over a thin distance, with weak effects when increasing De.

Besides inertial migration, cross-streamline migration of particles can occur in a sheared viscoelastic liquid due to the normal stresses arising in the suspending medium[9]. As for the case of the Carreau-Yasuda suspending liquid presented in Sec. III A, we have verified that no lateral migration is observed in the simulations with viscoelastic liquids.
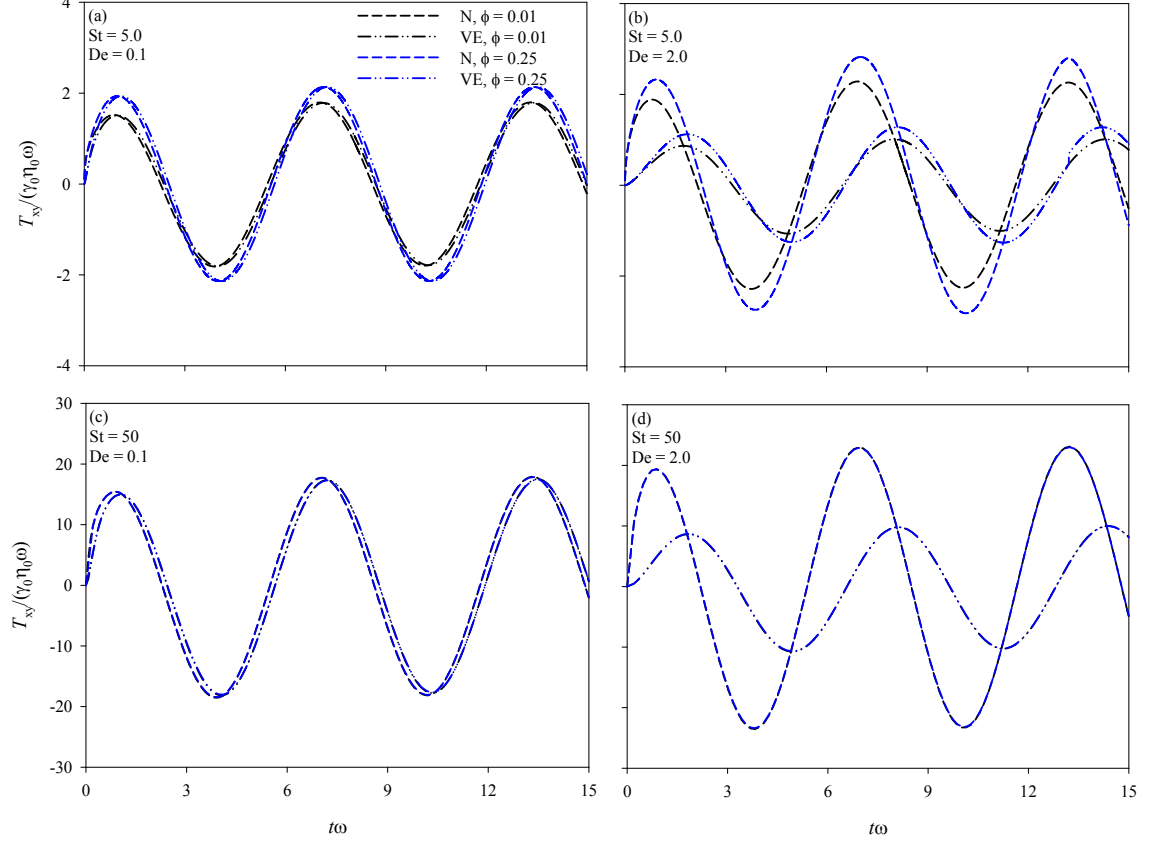
FIG. 12: Dynamics of the solvent (N) and polymer (VE) contributions to the shear stress in a suspension of mono-disperse non-colloidal rigid spheres in a Giesekus liquid with $\alpha = 0.125$ and $\beta = 0.5$ subjected to SAOS flow at four $\text{St}^{1/2} - \text{De}$ couples, as indicated in the legend, and for $\phi = 0.01, 0.25$.

In order to make a direct comparison between the results pertaining suspensions with rheologically different suspending liquids, we show in Fig. 15 the storage modulus (on the left) and the loss modulus (on the right) of suspensions with a Carreau-Yasuda and a Giesekus matrix as function of the dimensionless number expressing the ratio of the fluid and the flow characteristic times, i.e., Cu and De. For both constitutive equations, a dilute case with $\phi = 0.01$ and a concentrated case with $\phi = 0.25$ are considered. Of course, the data for the two fluids coincide at vanishing Cu/De, as these are representative of a suspension with a Newtonian matrix. On the top row of Fig. 15, $\text{St}^{1/2}$ is equal to 1.0. Concerning the storage modulus (see panel a1), the trends for a Carreau-Yasuda suspending liquid are horizontal. On the other hand, at low ϕ, the storage modulus of a Giesekus suspension overcomes that of a Carreau-Yasuda suspension at low Cu/De, then it crosses and goes increasingly below it at increasing Cu/De. At high ϕ, G' is always lower in a Giesekus suspension than in a Carreau-Yasuda suspension, with their quantitative difference that increases at increasing Cu/De. Instead, the loss modulus of a Giesekus suspension exhibits a way more pronounced thinning than that

of a Carreau-Yasuda suspension both in the dilute and the concentrated regime, as shown in panel a2. At high $\text{St}^{1/2} = 50$, the storage modulus of a Giesekus suspension stays above that of a Carreau-Yasuda suspension for $\text{Cu/De} \lesssim 1$, then the curves cross each other and the storage modulus of a Giesekus suspension becomes lower than that of a Carreau-Yasuda suspension at the same Cu/De (see panel b1). It can be also seen that the slope of the decreasing curves at high Cu/De is the same for the two fluids. Concerning the loss modulus, shown in panel b2, G'' is always larger in a Giesekus suspension than in a Carreau-Yasuda suspension, yet, beyond the maximum, the loss modulus curve for a Giesekus suspension attains a slope that would make it overlap that for a Carreau-Yasuda suspension at high Cu/De. For both the fluids and the moduli, the effect of the particle volume fraction is almost negligible at high $\text{St}^{1/2}$.

Let us now discuss the effects of the mobility parameter, α, and of the viscosity ratio, β, on the computationally measured storage and loss moduli of a suspension of mono-disperse non-colloidal rigid spheres in a viscoelastic liquid. Concerning α, we have performed the same set of simulations whose results are shown above also at $\alpha =$
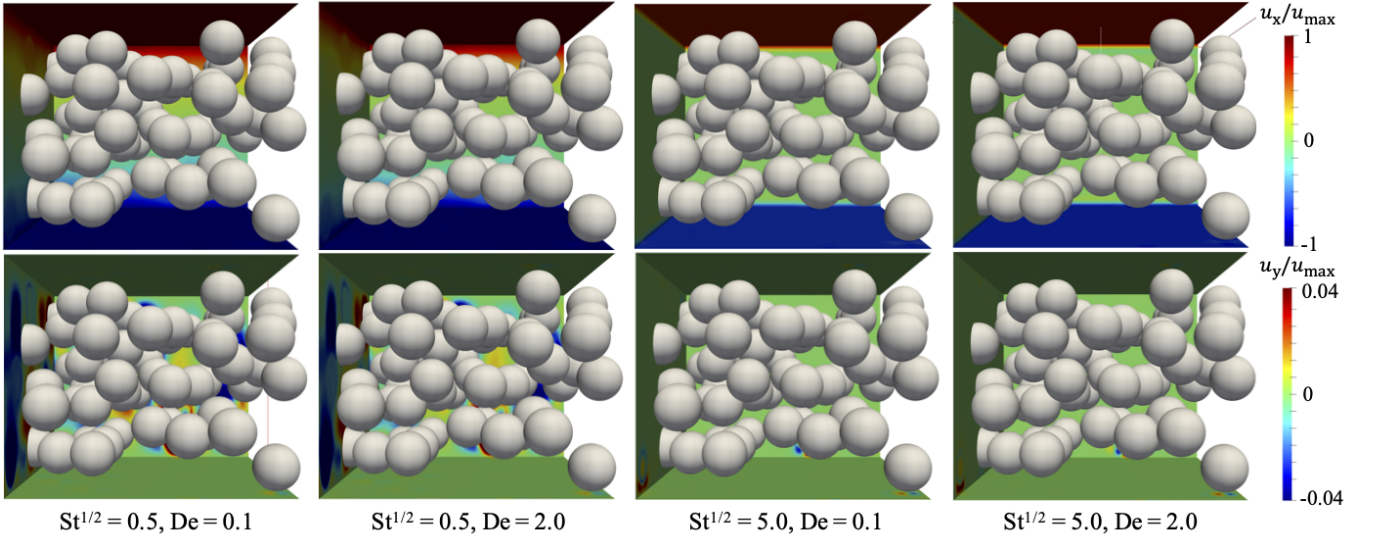
FIG. 13: Particle distribution and maps of the fluid dimensionless streamwise (top) and wall-normal (bottom) velocity on the moving walls, the xy-plane at $z = 0$, and the yz-plane at $x = 0$ for a suspension of mono-disperse non-colloidal rigid spheres with $\phi = 0.15$ in a Giesekus liquid with $\alpha = 0.125$ and $\beta = 0.5$ subjected to SAOS flow. Four $\mathrm{St}^{1/2} - \mathrm{De}$ combinations are considered. The snapshots refer to $t\omega = 5\pi/2$, the velocity-values are normalized by the maximum oscillatory velocity of the walls, $u_{\max} = (H/2)\gamma_0\omega$.
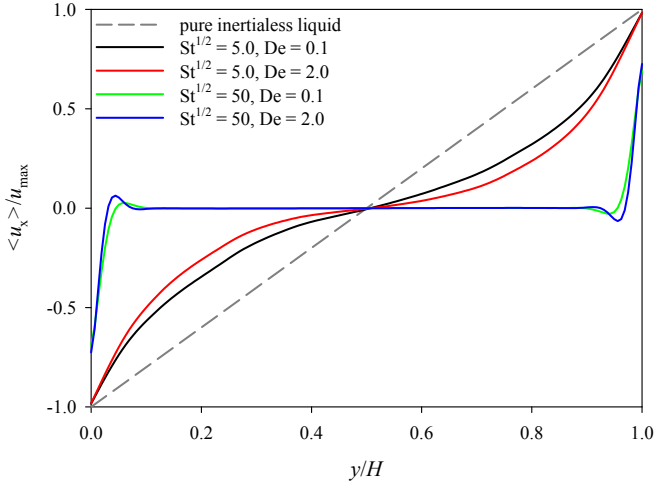

FIG. 14: Vertical profiles of the xz-surface average of the fluid dimensionless streamwise velocity in a suspension of mono-disperse non-colloidal rigid spheres with $\phi = 0.15$ in a Giesekus liquid with $\alpha = 0.125$ and $\beta = 0.5$ subjected to SAOS flow. Four $\mathrm{St}^{1/2} - \mathrm{De}$ combinations are considered, as indicated in the legend. The profiles refer to $t\omega = 5\pi/2$ and the velocity-values are normalized by the maximum oscillatory velocity of the walls, $u_{\max} = (H/2)\gamma_0\omega$.

0.25, thus for a 'more shear-thinning' Giesekus suspending liquid, and at $\alpha = 0$, namely, for a constant-viscosity Oldroyd-B matrix. For all the considered values of St, De,

and ϕ, the differences in the results obtained at varying α are so little that they are indistinguishable from those at $\alpha = 0.125$. For this reason, they are not reported in this paper. This would be expected for a pure inertialess Giesekus liquid, since its storage and loss moduli do not depend on α, as shown in Fig. 2b; apparently, neither non-negligible inertia nor the presence of the particles do modify this scenario. On the other hand, we show in Fig. 16 some results elucidating the effects of β. In particular, the top row reports the trends of $G'/(\eta_0\omega)$ (on the left) and $G''/(\eta_0\omega)$ (on the right) as a function of De at $\mathrm{St}^{1/2} = 5.0$ and for the four $\phi - \beta$ couples indicated in the legend. It can be observed that the behavior of the storage and loss moduli as a function of De does not change qualitatively when β is lowered from 0.5 to 0.2, yet there is an appreciable quantitative effect: indeed, given ϕ, both the moduli are increased with respect to their values at $\beta = 0.5$ when De is low, whereas they go below their values at $\beta = 0.5$ when De is high. On the bottom row of Fig. 16, we report the suspension storage and loss moduli as a function of De at $\mathrm{St}^{1/2} = 50$. At such high St, the value of G' and G'' at $\beta = 0.2$ is greater than the corresponding value at $\beta = 0.5$ (at the same De and ϕ). In addition, it should be remarked that, when $\mathrm{St}^{1/2} = 50$, the values of G' and G'' at different ϕ collapse even at $\beta = 0.2$.

As indicated in Sec. II, all the numerical results reported in this paper are obtained with a confinement ratio $D_p/H = 0.2$. In order to verify the possible occurrence of confinement effects, we plot in Fig. 17 the suspension moduli as a function of D_p/H for a Carreau-Yasuda matrix (panel a) and a Giesekus matrix with $\alpha = 0.125$ and
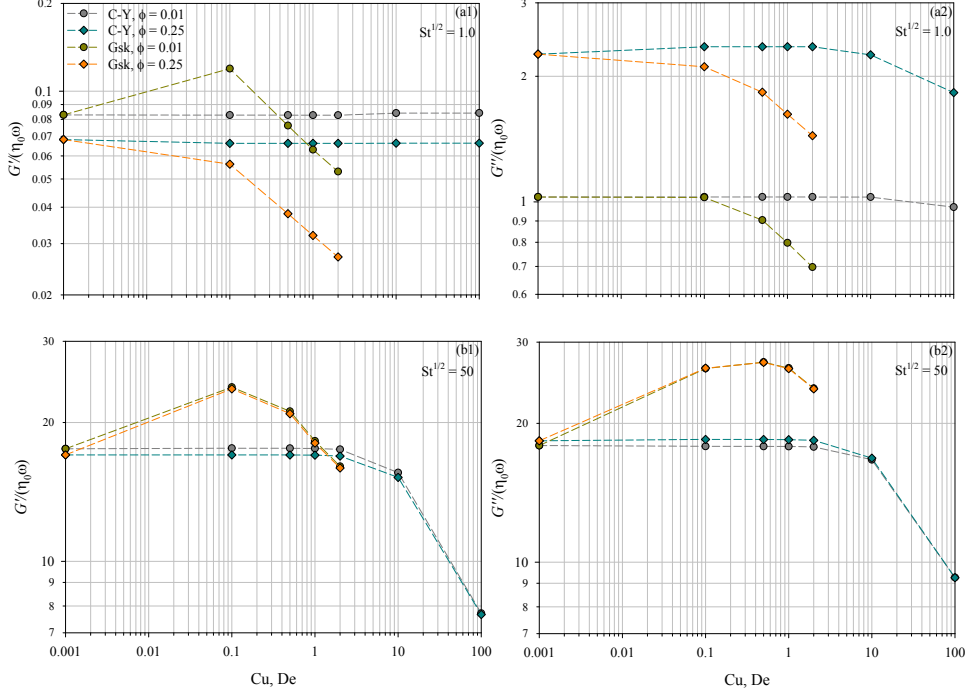
FIG. 15: Dimensionless storage modulus $G'/(\eta_0\omega)$ (left column) and loss modulus $G''/(\eta_0\omega)$ (right column) as a function of Cu for a suspension of mono-disperse non-colloidal rigid spheres in a Carreau-Yasuda liquid subjected to SAOS flow and as a function of De for a suspension with a Giesekus matrix with $\alpha = 0.125$ and $\beta = 0.5$. The data pertain the different values of the particle volume fraction, ϕ, indicated in the legend. Each row corresponds to a different value of the square root of the Stokes number, $St^{1/2}$, as indicated in the panels. The lines connecting the data have the scope of guiding the eye. The data at De = 0.001 correspond to a Newtonian suspending liquid and are conventionally attributed to such De for visualization purposes.

$\beta = 0.5$ (panel b). In both panels, the particle volume fraction is $\phi = 0.15$ and four $St^{1/2}$ - Cu (or De) combinations are considered. As the trends shown in Fig. 17 are all horizontal, we can infer that there are no particle confinement effects on the measured storage and loss moduli for $D_p/H \leq 0.2$. This is also a proof that our results do not depend on the randomly-chosen initial distribution of the particles. Indeed, different initial configurations of the system are considered when D_p/H is changed at given ϕ.

IV. CONCLUSIONS

In this paper, we investigate through interface-resolved numerical simulations the SAOS flow of suspensions of mono-disperse non-colloidal rigid spherical particles in non-Newtonian liquids from the dilute to the concentrated regime. We consider both an inelastic shear-thinning matrix, modeled by the Carreau-Yasuda constitutive equation, and viscoelastic matrices, modeled by the Giesekus and Oldroyd-B constitutive equations. Our simulations aim at elucidating the effects of the interplay among inertia, suspending liquid rheology, and particle concen-

tration on the measured storage and loss moduli of the suspensions.

Like in suspensions with a Newtonian matrix[32], in suspensions with a Carreau-Yasuda inelastic suspending liquid a non-zero storage modulus is always detected when inertia, measured by the Stokes number, St, is not zero. In particular, G' significantly increases with St, whereas it only moderately changes with the concentration of the solid phase. On the other hand, increasing the characteristic time of the Carreau liquid has almost no effect on G' until the product between such characteristic time and the oscillatory frequency, i.e., the Carreau number, Cu, reaches order unity, above which a significant decrease of the suspension storage modulus occurs, namely, increasing Cu hinders the suspension apparent elasticity. The loss modulus, G'', increases with both St and ϕ. Concerning the effect of Cu, there are no deviations of the loss modulus of a suspension with a Carreau-Yasuda matrix from that of a suspension with a Newtonian matrix below $\mathcal{O}(Cu) = 1$, whereas a significant decrease of G'' occurs when Cu is above $\mathcal{O}(10)$.

In suspensions with a Giesekus viscoelastic matrix, the storage modulus increases by orders of magnitude with St as an effect of the increasing apparent elasticity provided
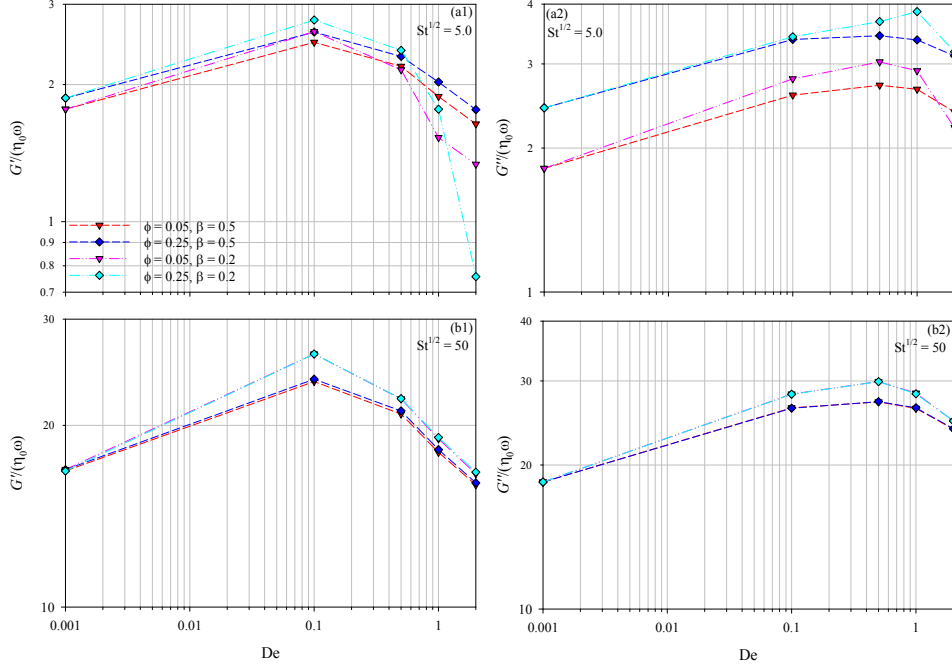
FIG. 16: Dimensionless storage modulus $G'/(\eta_0\omega)$ (left column) and loss modulus $G''/(\eta_0\omega)$ (right column) as a function of De for a suspension of mono-disperse non-colloidal rigid spheres in a Giesekus liquid with $\alpha = 0.125$ subjected to SAOS flow. Top row: $St^{1/2} = 5.0$; bottom row: $St^{1/2} = 50$. The data pertain the different values of the particle volume fraction, ϕ, and of the viscosity ratio, β, indicated in the legend. The lines connecting the data have the scope of guiding the eye. The data at De = 0.001 correspond to a Newtonian suspending liquid and are conventionally attributed to such De for visualization purposes.

by inertia[32], whereas it has a non-monotonic behavior passing through a maximum when increasing the ratio of the fluid relaxation time and the flow characteristic time, i.e., the Deborah number, De. On the other hand, G'' increases with St. Concerning the effect of De, the loss modulus decreases with it at low St, whereas it has a non-monotonic behavior passing through a maximum at moderate and high St. The effect of the concentration of the particles on both the moduli is progressively weaker at increasing inertia, with data at different ϕ collapsing at high St.

By making a direct quantitative comparison between the results for suspensions with Carreau-Yasuda and Giesekus matrices as a function of Cu and De, respectively, some relevant differences arise depending on the weight of inertia. Indeed, at high St, both the moduli of a Giesekus suspension overcome those of a Carreau-Yasuda suspension for a wide window of Cu/De, whereas, at low St, the moduli of a Giesekus suspension are generally lower than those of a Carreau-Yasuda suspension, the extent of the difference depending on Cu/De.

For suspensions with both Carreau-Yasuda and Giesekus matrices, the behavior of the moduli finds correspondence in the observation of the fluid velocity profiles at varying St and Cu/De, which, in turn, reflect on the shear stress curves. In particular, the profile of the fluid streamwise velocity in the vertical direction becomes non-linear when inertia is non-negligible, consequently modifying the shear rate profile. Even, at high St the fluid is almost still in a wide region at the center of the channel gap and the streamwise velocity goes to the wall value to almost zero in two narrow regions close to the moving walls. Changing Cu/De quantitatively affects such profiles.

Since the Giesekus constitutive equation predicts both viscoelasticity and shear-thinning, the influence of the extent of the latter on the suspension moduli is investigated by considering both a 'more shear-thinning' Giesekus matrix and a constant-viscosity Oldroyd-B suspending liquid, yet no appreciable effects are detected, thus reproducing the behavior predicted by the constitutive equation for a pure inertialess liquid. On the contrary, changing the relative importance of the 'solvent' and 'polymer' contributions to the suspension matrix viscosity has a quantitative effect on the computationally measured G' and G''. In particular, at high St, lowering β enhances both the storage and the loss modulus regardless of De, whereas, at low St, lowering β makes the moduli increase at low De and decrease at high De.

[1] Alghalibi, D., Fornari, W., Rosti, M. E., and Brandt, L., International Journal of Multiphase Flow , 103291 (2020).

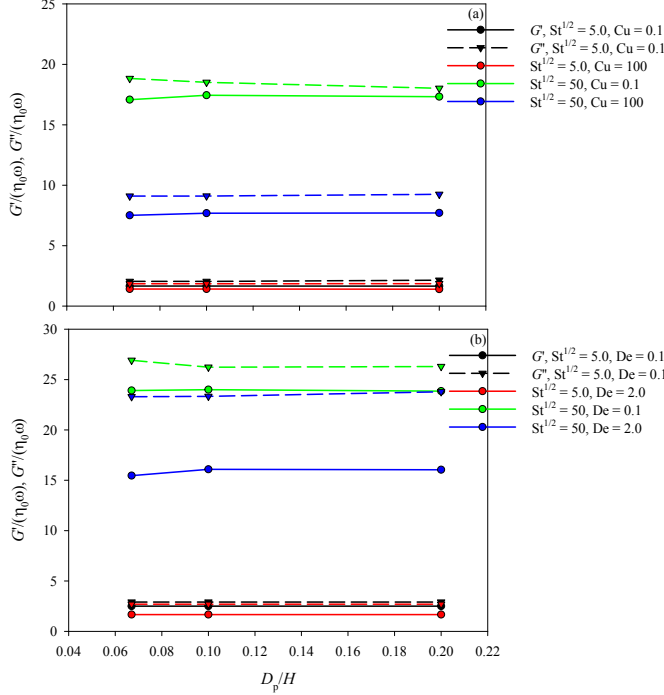FIG. 17: Dimensionless storage modulus, $G'/(\eta_0\omega)$, and loss modulus, $G''/(\eta_0\omega)$, as a function of D_p/H for a suspension of mono-disperse non-colloidal rigid spheres with volume fraction $\phi = 0.15$ in a Carreau-Yasuda liquid (a) and in a Giesekus liquid with $\alpha = 0.125$ and $\beta = 0.5$ (b) subjected to SAOS flow. Four $St^{1/2}$ - Cu (or De) couples are considered, as indicated in the legend. The lines connecting the data have the scope of guiding the eye.

[2] Alghalibi, D., Lashgari, I., Brandt, L., and Hormozi, S., Journal of Fluid Mechanics **852**, 329 (2018).

[3] Barnes, H. A., Rheology Reviews , 1 (2003).

[4] Bird, R. B., Armstrong, R. C., and Hassager, O., *Dynamics of polymeric liquids. Vol. 1: Fluid mechanics* (Wiley, New York, 1987).

[5] Böhme, G.and Stenger, M., Journal of Rheology **34**, 415 (1990).

[6] Breugem, W.-P., Journal of Computational Physics **231**, 4469 (2012).

[7] Costa, P., Boersma, B. J., Westerweel, J., and Breugem, W.-P., Physical Review E **92**, 053012 (2015).

[8] D'Avino, G., Greco, F., Hulsen, M. A., and Maffettone, P. L., Journal of Rheology **57**, 813 (2013).

[9] D'Avino, G., Maffettone, P. L., Greco, F., and Hulsen, M. A., Journal of Non-Newtonian Fluid Mechanics **165**, 466 (2010).

[10] Einstein, A., Annalen der Physik **339**, 591 (1911).

[11] Ferry, J. D., *Viscoelastic properties of polymers* (John Wiley & Sons, 1980).

[12] Gallier, S., Lemaire, E., Peters, F., and Lobry, L., Journal of Fluid Mechanics **757**, 514 (2014).

[13] Izbassarov, D., Rosti, M. E., Ardekani, M. N., Sarabian, M., Hormozi, S., Brandt, L., and Tammisola, O., International Journal for Numerical Methods in Fluids **88**, 521 (2018).

[14] Kim, J.and Moin, P., Journal of Computational Physics **59**, 308 (1985).

[15] Larson, R. G., *Constitutive equations for polymer melts and solutions: Butterworths series in chemical engineering* (Butterworth-Heinemann, Boston, 2013).

[16] Macosko, C. W.and Larson, R. G., *Rheology: principles, measurements, and applications* (Vch, New York, 1994).

[17] Mahmud, A., Dai, S., and Tanner, R. I., Journal of Rheology **64**, 1087 (2020).

[18] Matsuoka, Y., Nakayama, Y., and Kajiwara, T., Soft Matter **16**, 728 (2020).

[19] Matsuoka, Y., Nakayama, Y., and Kajiwara, T., Journal of Fluid Mechanics **913** (2021).

[20] McLaughlin, J. B., Journal of Fluid Mechanics **246**, 249 (1993).

[21] Metzner, A., Journal of Rheology **29**, 739 (1985).

[22] Mewis, J.and Wagner, N. J., Journal of Non-Newtonian Fluid Mechanics **157**, 147 (2009).

[23] Picano, F., Breugem, W.-P., Mitra, D., and Brandt, L., Physical Review Letters **111**, 098302 (2013).

[24] Rosti, M. E., Ardekani, M. N., and Brandt, L., Physical Review Fluids **4**, 062301 (2019).

[25] Rosti, M. E.and Brandt, L., Journal of Non-Newtonian Fluid Mechanics **262**, 3 (2018).

[26] Rosti, M. E.and Brandt, L., Physical Review Fluids **5**, 041301 (2020).

[27] Rosti, M. E., Mirbod, P., and Brandt, L., Chemical Engineering Science **230**, 116178 (2020).

[28] Shaqfeh, E. S., AIChE Journal **65**, e16575 (2019).

[29] Tanner, R. I., Physics of Fluids **30**, 101301 (2018).

[30] Tanner, R. I., Journal of Rheology **63**, 705 (2019).

[31] Vázquez-Quesada, A., Español, P., Tanner, R. I., and Ellero, M., Journal of Fluid Mechanics (2019).

[32] Villone, M. M., Rosti, M. E., Tammisola, O., and Brandt, L., Rheologica Acta **58**, 741 (2019).

[33] Yang, M., Krishnan, S., and Shaqfeh, E. S., Journal of Non-Newtonian Fluid Mechanics **233**, 181 (2016).

[34] Yang, M.and Shaqfeh, E. S., Journal of Rheology **62**, 1363 (2018).